Nanoscale

Accepted Manuscript

This article can be cited before page numbers have been issued, to do this please use: N. Puthumadathil, S. Krishnan R, G. S. Nair and M. R. Kozhinjampara, *Nanoscale*, 2022, DOI: 10.1039/D2NR00556E.

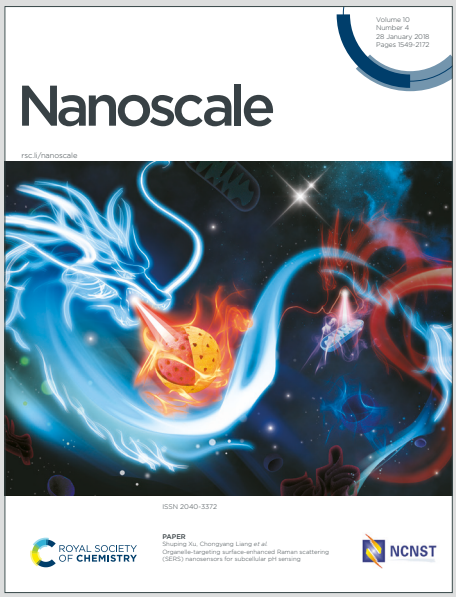

ROYAL SOCIETY OF CHEMISTRY

rsc.li/nanoscale

View Article Online
DOI: 10.1039/D2NR00556E

Assembly of alpha-helical transmembrane pores through the intermediate state

Neethu Puthumadathil[1,2†], Smrithi R Krishnan[1,2†], Greeshma S Nair[1], and Kozhinjampara R Mahendran[1]*

[†]Contributed equally to this work

[1]Membrane Biology Laboratory, Transdisciplinary Research Program, Rajiv Gandhi Centre for Biotechnology, Thiruvananthapuram 695014, India.

[2]Manipal Academy of Higher Education, Manipal, Karnataka, India-576104

*To whom correspondence should be addressed

*e-mail: mahendran@rgcb.res.in

View Article Online
DOI: 10.1039/D2NR00556E

Abstract

Pore-forming alpha-helical proteins are well known for their dynamic assembly mechanism and it has been challenging to delineate the pore-forming structures in the membrane. Previously, attempts have been made to elucidate their assembly mechanism and there is a large gap due to complex pathways by which these membrane-active pores impart their effect. Here we demonstrate the multi-step structural assembly pathway of alpha-helical peptide pores formed by a 37 amino-acid synthetic peptide, pPorU based on the natural porin from *Corynebacterium urealyticum* using single-channel electrical recordings. More specifically, we report detectable intermediates states during membrane insertion and pore formation of pPorU. The fully assembled pore exhibited unusually large stable conductance, voltage-dependent gating, and functional blockage by cyclic sugar generally applicable to a range of transmembrane pores. Furthermore, we used rationally designed mutants to understand the role of specific amino acids in the assembly of these peptide pores. Mutant peptides that differ from wild-type peptides produced noisy, unstable intermediate states and low conductance pores, demonstrating sequence specificity in the pore-formation process supported by molecular dynamics simulations. We suggest that our study contributes to understanding the mechanism of action of naturally occurring alpha-helical pore-forming proteins and should be of broad interest to build peptide-based nanopore sensors.

Keywords: Alpha-helical, pores, membrane, conductance, intermediate states, single-channel

View Article Online
DOI: 10.1039/D2NR00556E

Introduction

Membrane proteins carry out an extensive range of biological functions, including transport of ions, nutrients and metabolites, signal transduction, cell adhesion, anchoring other proteins, organizing organelles and cell shape.[1-3] There are two main structural classes of membrane proteins: alpha-helix and β barrels, where alpha-helices are more abundant than β-barrels.[1] One such class of membrane proteins, i.e., pore-forming toxins (PFTs), are essential virulence factors secreted as soluble monomers that assemble into a structured oligomeric functional pore at the target membranes.[4-7] Their mechanism of action involves the conversion of a prepore state to a pore via a complex assembly pathway comprising of transient intermediate steps.[4, 8-11] Importantly, understanding their discrete dynamic assembly mechanism is vital in the development of therapeutics.[7] Various techniques have been used to understand the assembly pathway of PFTs, including X-Ray crystallography, cryo-EM and fast-scan atomic force microscopy.[4, 7, 12, 13] Interestingly, PFTs undergo large conformational changes depending on their native environment and hence, it is important to use techniques that provide information on the assembly dynamics in real-time in the membrane.[4, 9]

Notably, single-channel electrical recording is a method of choice for the characterization of pore-forming proteins as it provides insights into their structural and functional properties in the membrane environment.[9, 14] Generally, the intermediate states for pore-forming proteins are electrically silent with non-conducting states, and these states are most likely short-lived. [8, 9, 15] In addition to their potential in the development of therapeutics, certain PFTs such as α-hemolysin, ClyA, FraC, aerolysin have been used as nanopore sensors due to their unique architecture and pore geometry.[16-23] Remarkably, there is great interest in developing large pores formed from short synthetic peptides and DNA nanostructures.[24] Alpha-helical pore assemblies are particularly

View Article Online
DOI: 10.1039/D2NR00556E

exciting targets due to their similarities to natural ion channels.[25-28] Notably, there are many obstacles in understanding alpha-helical assemblies due to their complex refolding mechanism and non-specific interactions with the membrane.[29-31] Previously, we assembled a large synthetic transmembrane pore from 40-amino-acid alpha-helical peptides.[32] The pore is charge selective, functional and capable of conducting ions and binding blockers such as cyclic oligosaccharides.[32] We demonstrated the binding and translocation of differently charged peptides through these synthetic alpha-helical pores.[33]

Here, we report a synthetic transmembrane pore, pPorU, built from 37-amino-acid peptides, corresponding to natural pore PorACur derived from *Corynebacterium urealyticum*.[34] There were certain unique features to pPorU, including a tryptophan residue in the middle of the sequence compared to the terminal in other alpha-helical transmembrane motifs, proline and a cluster of phenylalanine residues resulting in further interest in the pore **(Fig. 1a and fig. S1)**. We probed the structure, assembly and conductance properties of these channels using a combination of peptide redesign and synthesis, solution-phase biophysics, single-channel recordings and molecular dynamics simulations. We observed well-defined intermediate states during membrane insertion and pore formation of amphipathic alpha-helices. We suggest these synthetic peptides can act as a template to provide a model for understanding the assembly pathway of large pores, such as that found in bacterial toxins, pore-forming proteins of the immune system and antimicrobial peptides.[4, 35-37] Our findings have important implications in biotechnology for designing pores for applications in nanopore technology and single-molecule nanopore chemistry.[25, 38]

View Article Online
DOI: 10.1039/D2NR00556E

Results and Discussion

Biophysical properties of pPorU peptides

The natural porin PorACur derived from *Corynebacterium urealyticum* is a membrane-spanning alpha-helical pore, and our goal was to see if a synthetic peptide based on this natural porin can spontaneously self-assemble into a pore in the membrane environment.[34] The 37 amino acid pPorU peptide was designed based on the sequence of natural porin PorACur and synthesized by solid-phase synthesis **(Fig. 1a)**.

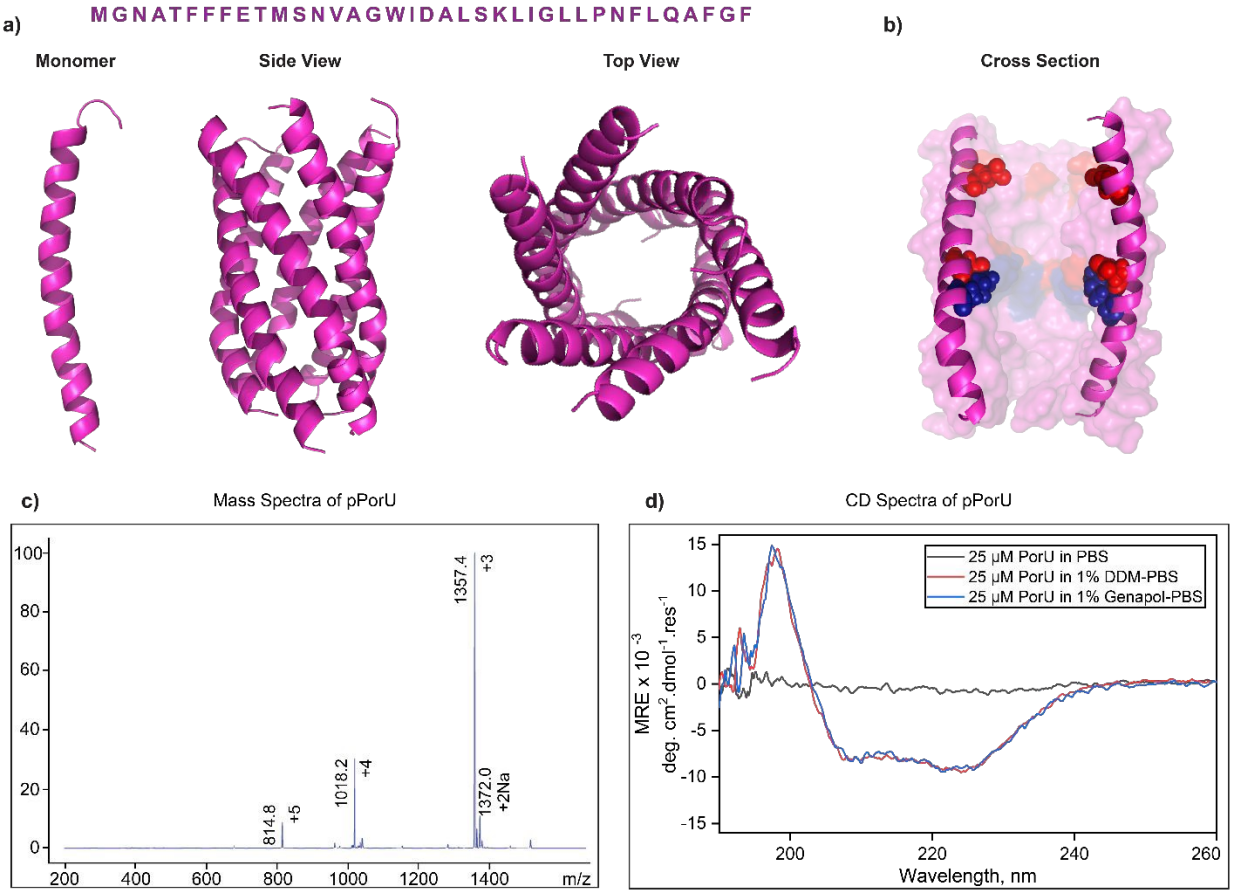

Fig. 1: Biophysical properties of pPorU peptides.

a) Modeled structure (Side view and Top view) and sequence of pPorU. **b)** Cross-sectional view of pPorU with positive residues in blue and negative residues in red. **c)** Mass spectra of pPorU peptide **d)** CD spectra of 25 µM pPorU in PBS (black), 1% DDM (red) and 1% Genapol (blue).

View Article Online
DOI: 10.1039/D2NR00556E

The structure of peptide pPorU pore is not available and here we show the modeled hexameric pPorU based on the natural porin PorACur constructed using the CCBuilder.[34] The modeled structure (**Fig. 1b**) shows the cross-section of the pore with its electrostatic distribution (positively charged residue in blue and negatively charged residues in red). Both positively charged residues and denser negatively charged residues line the lumen of the pore, which might act as a binding site for charged analytes and contribute to the charge selectivity of the pore. The peptides were purified by reverse-phase high-performance liquid chromatography (HPLC) and the mass of the peptide was confirmed using mass spectroscopy (**Fig. 1c**). Next, we investigated the secondary structure of the peptide using circular dichroism (CD) spectroscopy. A 25 μM peptide solution was prepared in different detergents such as 1% n-dodecyl-B-D-maltoside (DDM) and 1% Genapol solubilized in phosphate-buffered saline (PBS) (**Fig. 1d**). The peptide exists in random coil conformation in PBS and folds itself into an alpha-helix conformation in the presence of detergent micelles **(Fig. 1d)**.

Electrical properties of pPorU peptides

The peptide (pPorU) was solubilized in 0.1% DDM and introduced into 1,2-diphytanoyl-sn-glycero-3-phosphocholine (DPhPC) planar lipid bilayer for characterization using single-channel electrical recordings in electrolyte buffer (1 M KCl, 10 mM HEPES, pH 7.4). The insertion of pPorU peptides into DPhPC bilayers was studied at different voltages ranging from +50 mV to +270 mV **(Fig. 2, fig 5, fig. S2, fig. S3 and fig. S6)**. Remarkably, at a very high potential difference (≥ +200 mV), the pPorU peptide formed a large pore of stable conductance state in the lipid bilayers **(Fig. 2a, fig. S2 and fig. S3)**. Interestingly, the insertion of the peptides into the membrane occurred via an intermediate step (I), finally forming a large stable pore. (**Fig. 2a**). The (I) state is

View Article Online
DOI: 10.1039/D2NR00556E

an intermediate noisy conductance state, which exhibited slight current fluctuations, and this distinct conductance was calculated to be ~2 nS **(Fig. 2, fig. S2 and fig. S3).** This state mostly lasts for milliseconds, representing the pore continuing oligomerization in the membrane, opening into a large pore (L). The timeline for forming large stable pores from intermediate ranges from milliseconds to several seconds, resolved by single-channel recordings **(fig. S2)**.

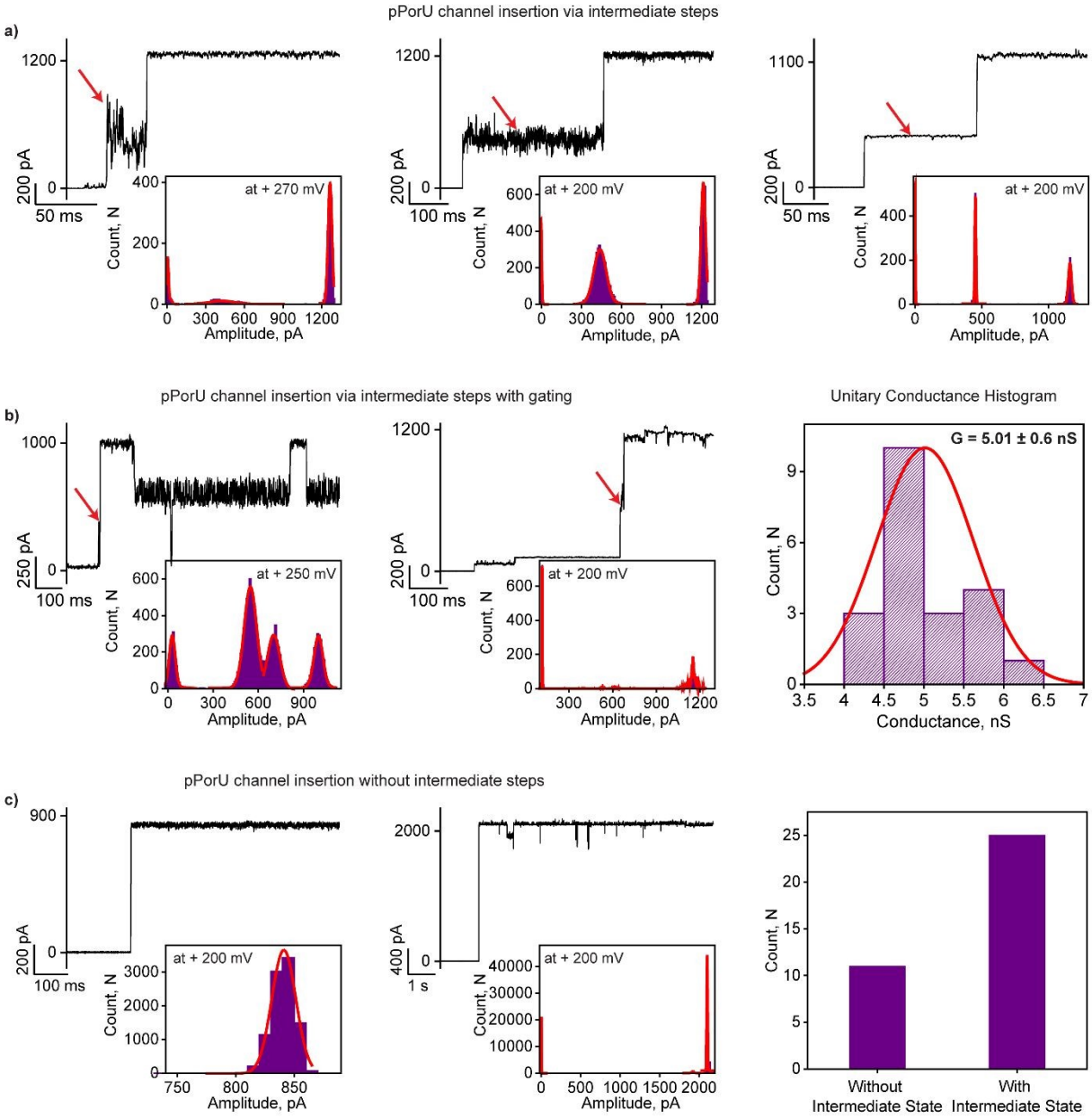

Fig. 2: Electrical properties of pPorU pore

View Article Online
DOI: 10.1039/D2NR00556E

a) Electrical recording of single pPorU channel insertions into DPhPC lipid bilayer at +270 mV and +200 mV via an intermediate step (red arrows). The corresponding current amplitude histogram is shown in inset. **b)** Electrical recording of single pPorU channel insertion into DPhPC lipid bilayer at +250 mV and +200 mV via an intermediate step showing gating. The corresponding current amplitude histogram is shown in inset. The unitary conductance histogram based on single-channel insertions forming large pores via the intermediate step shown here was obtained by fitting the distribution to a single Gaussian (n = 21). **c)** Electrical recordings of single pPorU channels without an intermediate state at +200 mV. A bar graph representing the distribution of pPorU channel insertions with and without the intermediate state is shown. The current signals were filtered at 2 kHz and sampled at 10 kHz. Electrolyte: 1 M KCl, 10 mM HEPES, pH 7.4.

Notably, numerous insertions of pPorU peptides were recorded and the transition into the large pore via the intermediate state was observed multiple times, specifically at higher voltages (**Fig. 2a** and **fig. S2**). During several insertion events, the L state showed ion current fluctuations owing to gating at higher voltages under which the channel inserts (**Fig. 2b**). Furthermore, a unitary conductance histogram was obtained based on the statistical analysis of single-channel insertion events of the large stable pores formed via an intermediate state. The mean unitary conductance of the large stable pore was calculated to be 5.01 ± 0,6 ns (n=21), indicating the formation of uniform pores in the membrane **(Fig. 2a-b, Fig. 3, fig. S2 and fig. S3)**. Additionally, we observed large pore formation devoid of the intermediate step and such pores had L states of varying conductance up to ~ 10 nS (**Fig. 2c and fig. S3**). This large conductance could be due to 2 individual L state pores in the membrane. We attribute this to the rapid pore assembly wherein the intermediate state could not be resolved in both cases**.** However, as evident from the bar graph, the incidence of pores with an intermediate is considerably higher than that of single-step channel insertions **(Fig. 2c).**

View Article Online
DOI: 10.1039/D2NR00556E

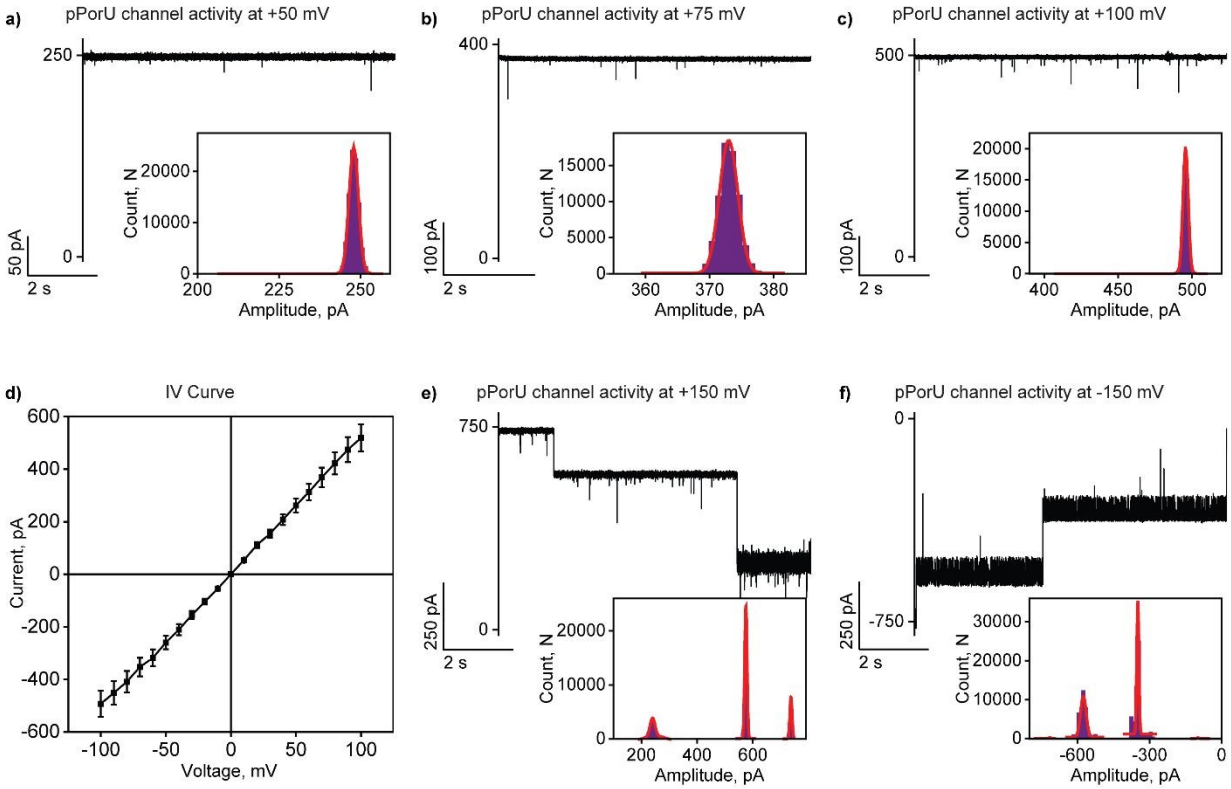

Fig. 3: Electrical properties of pPorU pore

a-c) Electrical recording of single pPorU pore (L state) at +50 mV, +75 mV and +100 mV with the corresponding current-amplitude histogram showing stable conductance state without gating. **d)** Current-Voltage curve is shown. **e-f)** Electrical recording of single pPorU pore (L state) at +150 mV and -150 mV with the corresponding current-amplitude histogram showing gating. The current signals were filtered at 2 kHz and sampled at 10 kHz. Electrolyte: 1 M KCl, 10 mM HEPES, pH 7.4.

Notably, pPorU (L state pores) exhibited voltage-dependent gating, which is the intrinsic property of the membrane pores and the threshold potential of gating varies from pore to pore. Significantly, after pore formation, gating was observed only at higher voltages (≥±150 mV), wherein the pore fluctuated between open and closed conductance states **(Fig. 3 and fig. S4).** In contrast, the pore remained in a stable open conductance of ~ 5.0 nS (1M KCl) at voltages up to ± 100 mV **(Fig. 3 and Sfig 4).** The threshold potential for gating of the pPorU pores is ± 150 mV based on 21

View Article Online
DOI: 10.1039/D2NR00556E

individual pPorU pores (L state) inserted into the membrane. We emphasize that this new class of alpha-helical pores is rare to show very large conductance and is advantageous over biological and DNA pores.[17, 24] . The characterization of pores with a short polypeptide sequence is essential for sensing because such peptides can be made chemically and readily inserted into lipid bilayers. It is essential for all new pores, biological or engineered, to show that ion flow is through the expected pathway. One approach is to block the ion current through the pore using blockers to deduce the functional properties of the pore. We highlight that the pPorU pore lumen is lined by abundant negatively charged residues that act as an affinity site to facilitate the binding of cationic molecules. We also suggest that the larger conductance pore formed by pPorU peptides can be used as a nanopore sensor for single-molecule sensing of analytes **(Fig. 4 and fig. S5)**.

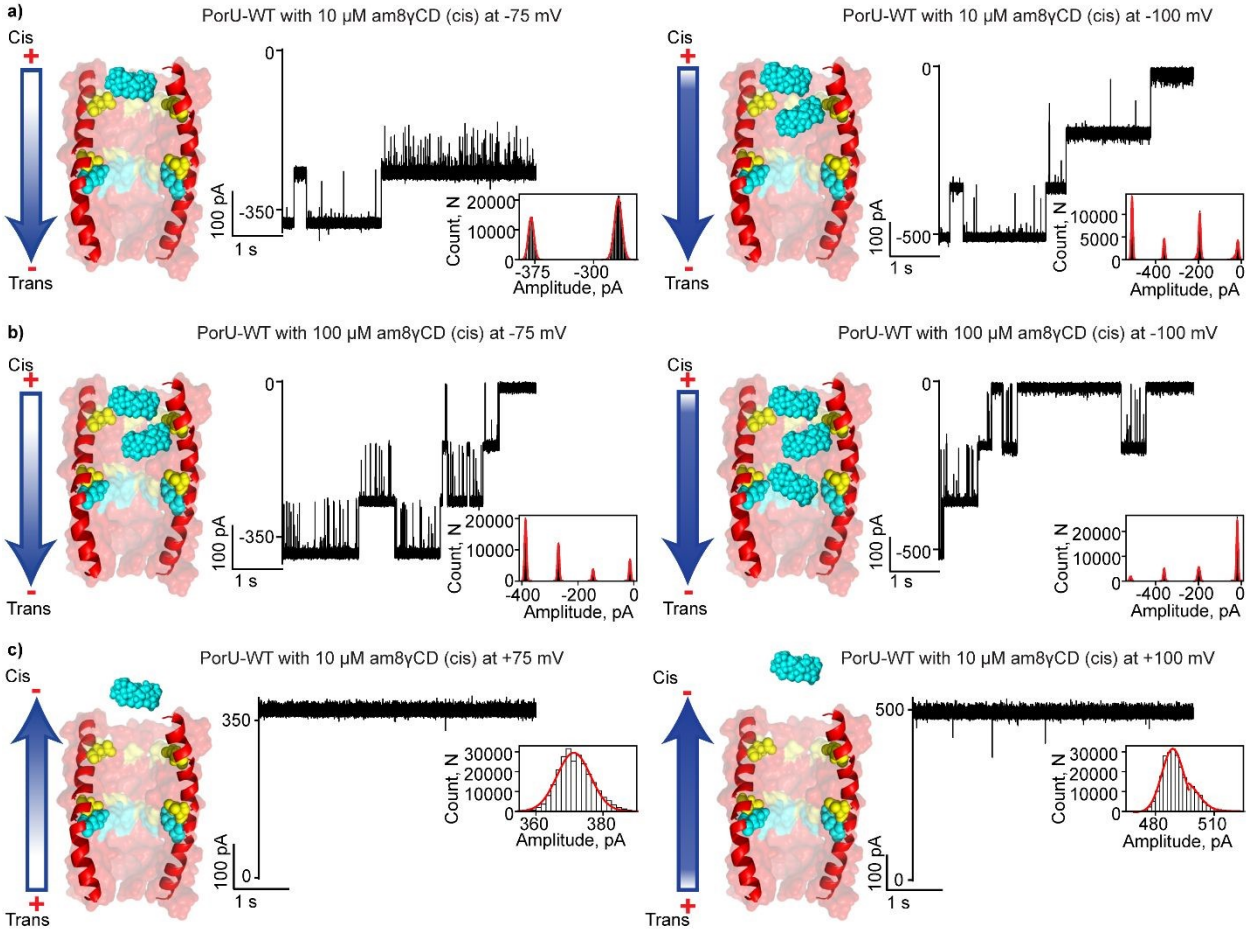

View Article Online
DOI: 10.1039/D2NR00556E

Figure 4: Interaction of pPorU pore with cationic cyclodextrin

a) Electrical recordings showing the interaction of cationic gamma cyclodextrin ($am_8\gamma CD$) with single pPorU pore (10 μM, cis) at -75 mV and -100 mV. **b)** Electrical recordings the interaction of cationic gamma cyclodextrin ($am_8\gamma CD$) with single pPorU pore (100 μM, cis) at -75 mV and -100 mV. **c)** Electrical recordings showing the interaction of cationic gamma cyclodextrin ($am_8\gamma CD$) with single pPorU pore (10 μM, cis) at +75 mV and +100 mV. The corresponding amplitude histogram is shown in the inset. Current signals were filtered at 10 kHz and sampled at 50 kHz. Electrolyte: 1 M KCl, 10 mM HEPES, pH 7.4.

Accordingly, we examined the interaction of cationic cyclodextrins ($am_8\gamma CD$) with pPorU peptide pores to demonstrate the functional properties of the pore. More specifically, we studied the selective binding of cationic CD, $am_8\gamma CD$, with pPorU in a voltage-dependent and concentration-dependent manner. The addition of 10 μM $am_8\gamma CD$ to the cis side resulted in ionic current blockages at negative voltages as CDs are electrophoretically driven through the pore, promoting electrostatic interactions with negatively charged residues **(Fig. 4a)**. Importantly, $am_8\gamma CD$ blocked the pore in a voltage-dependent manner. For example, at -50 mV, the pore remained in an open state and at -75 mV, $am_8\gamma CD$ blocked the pore strongly, resulting in the ion current blockages in steps without reverting to an open state. Further, an increase in the voltage to -100 mV resulted in a more rapid pore closure in multiple steps, indicating different CD binding sites in the pore **(Table S1).** No blockages were observed at positive voltages suggesting electrostatic repulsion of CDs. Based on this, we suggest that the applied voltage serves as a driving force facilitating the pulling and binding of the cationic CDs into the pore. Next, we increased the concentration of CDs to 100 μM (cis side), resulting in rapid pore-blocking at negative voltages. For example, $am_8\gamma CD$ blocked the pore even at -50 mV and more rapid pore closure was observed at increasing voltages (-75 mV

View Article Online
DOI: 10.1039/D2NR00556E

and -100 mV). We show that the higher concentration of the CDs rapidly blocks the pore more rapidly, indicating strong electrostatic interaction **(Fig. 4b)**.

Next, we perfused the CDs added to the cis side and then added $am_8\gamma CD$ to the trans side of the same pore so that the similar orientation of the pore was maintained. The addition of 10 μM $am_8\gamma CD$ to the trans side resulted in current blockades at positive potentials in agreement with electrophoretic binding of the CDs **(fig. S5)**. The pore remained open at lower voltages and $am_8\gamma CD$ blocked the pore at voltages above +50 mV. The binding of cationic CDs suggests the distribution of negatively charged residues along the pore surface that serves as a binding site for electrostatic interaction between the cationic CDs and negatively charged residues. Based on this data, we propose that the dense negative charge pattern inside the pore lumen can be exploited to develop a nanopore sensor for single-molecule sensing.

Following this, the insertion of pPorU peptides into planar lipid membranes was studied at lower voltages (±50 mV and ±100 mV) and surprisingly, large-conductance pore formation was not detected irrespective of different concentrations of the pPorU peptides added into the bilayer chamber **(Fig. 5a-5c and fig. S6).** At lower voltages (+50 mV and +100 mV), pPorU peptides formed fluctuating pores of low conductance states, indicating heterogeneous forms in the membrane **(Fig. 5a-5c and fig. S6).** Specifically, we observed two distinct pore populations and the pore conductance fluctuated between open and closed states. We observed that peptides formed transient spikes and fluctuating low conductance pores (5-50 pA), referred to as low conductance state. In some instances, the peptides formed pores with properties similar to the intermediate state (I) (~ 2 nS in 1M KCl), which fluctuated between several sub conductance states **(Fig. 5b and fig.**

View Article Online
DOI: 10.1039/D2NR00556E

S6). However, the pore remained either low conductance or intermediate (I) state and did not open into a large stable conductance state (L) at lower voltages.

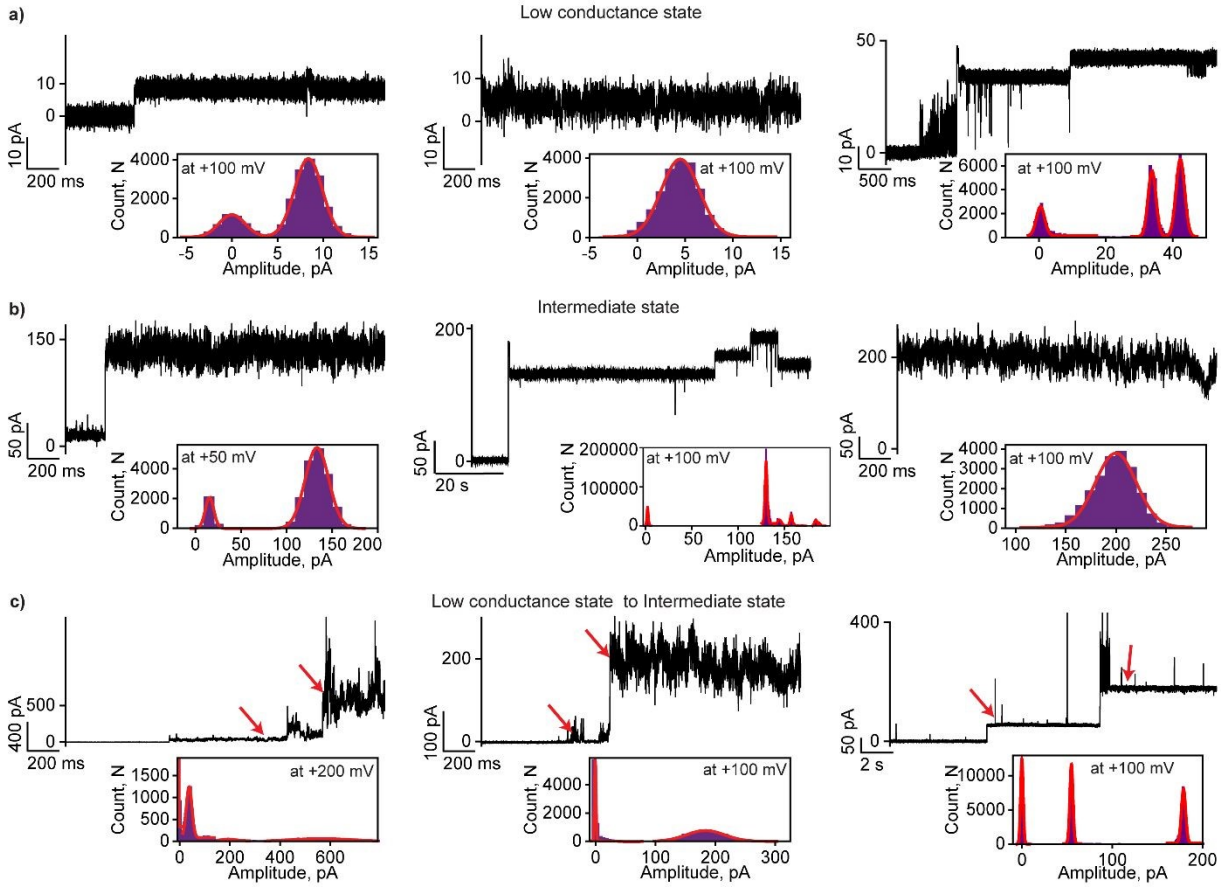

Fig. 5: Electrical properties of pPorU pore

a) Electrical recording of low conductance states at lower voltages inserted into the lipid membrane at +100 mV. **b)** Electrical recording of different intermediate states at lower voltages showing higher conductance states inserted at +50 mV and +100 mV. **c)** Electrical recording of intermediate states at lower voltages shows the transition of different conductance states at +100 mV and +200 mV. The corresponding amplitude histogram is shown in the inset. Current signals were filtered at 2 kHz and sampled at 10 kHz. Electrolyte: 1 M KCl, 10 mM HEPES, pH 7.4.

Thus, we showed that the pPorU peptide interaction with the membrane could be trapped in the intermediates steps by applying lower potential during pore insertion, allowing characterization of the assembly pathway. This indicates that the pPorU peptides are not assembled into stable

View Article Online
DOI: 10.1039/D2NR00556E

oligomers in the membrane at lower voltages **(Fig. 5 and fig. S6).** In comparison, higher voltages induce the formation of a large stable pore in the membrane via intermediates.

The specificity of pore assembly: pPorU mutants

To elucidate the pore assembly pathway based on the time-resolved intermediate states detected during pPorU peptide insertions, we rationally designed mutant peptides based on the modeled pPorU. We specifically designed two mutants, pPorU-W17C and pPorU-P29C, to understand the role of these amino acids in the assembly of alpha-helical peptide pores (**Fig. 6, fig. S7, and fig. S8**).

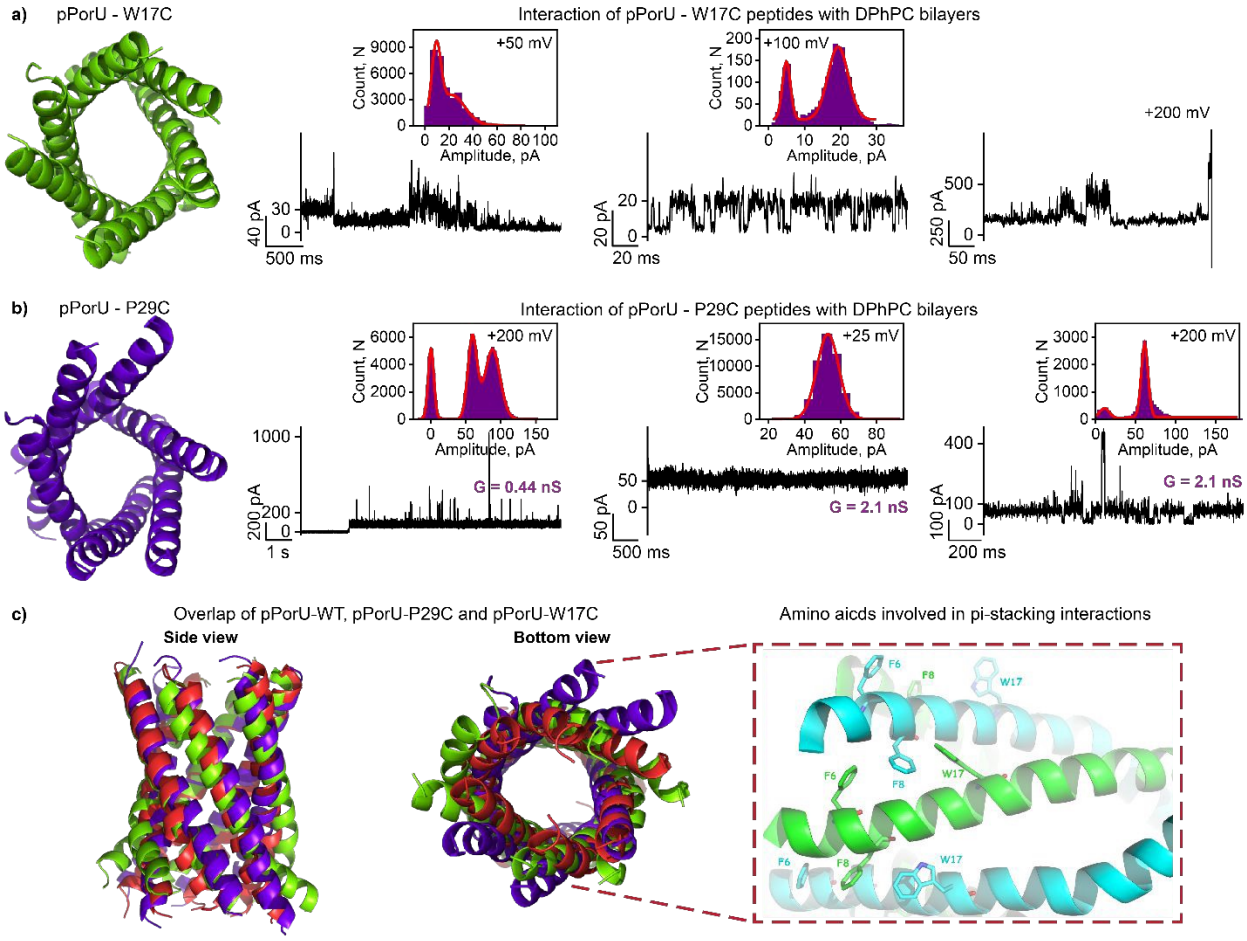

Fig. 6: pPorU mutants and molecular dynamics simulations of pPorU pores

View Article Online
DOI: 10.1039/D2NR00556E

a) Modeled structure of pPorU-W17C. Electrical recording of pPorU-W17C peptides showing fluctuations at +50 mV. Electrical recording of the pPorU-W17C peptides showing two states at +100 mV and bilayer disruption at +200 mV. **b)** Modeled structure of pPorU-P29C. Electrical recordings of pPorU-P29C showing low conductance channel activity at +200 mV and +25 mV. The corresponding amplitude histogram is shown in the inset. Current signals were filtered at 2 kHz and sampled at 10 kHz. Electrolyte: 1 M KCl, 10 mM HEPES, pH 7.4. **c)** Modelled hexameric pPorU-WT (red) overlapped with pPorU-W17C (green) and pPorU-P29C (blue). Side view of the WT pPorU structure, showing critical residues involved in a regular series of pi-stacking interactions that stabilize the N-terminal portion of the pore (Right).

Tryptophan residues, present predominantly in membrane proteins than soluble proteins, have been predicted to play an important role in anchoring pores in the membrane.[39, 40] Further, the presence of tryptophan in the middle of the pPorU sequence in contrast to the terminal position as located in other membrane proteins, including antimicrobial peptides, stimulated us to focus on this particular amino acid. The second residue of interest, proline, has been known to form kinks in the secondary structure of peptides and proteins.[41-43] Previous studies have shown that proline residues in membrane proteins (transmembrane alpha-helices) induce distortions and play a key role in helix packing, thus contributing to dynamic flexibility.[44-47] In this study, both the mutant peptides were designed by substituting the respective amino acids with cysteine. Cysteine was engineered to deduce the subunit composition of the pore using site-specific chemical modification in single-channel recordings, as shown previously.[28,32] The peptides pPorU-W17C and pPorU-P29C were synthesized by solid-phase synthesis and purified similar to WT pPorU by HPLC and the mass of the peptides was confirmed using mass spectroscopy **(fig. S7 and fig. S8)**. Accordingly, we examined the pore-forming properties of the mutant peptides using single-channel electrical recordings. The insertion of pPorU-W17C peptides was studied at lower and higher voltages (+200 mV) **(Fig. 6a and fig. S7)**. The mutant pPorU-W17C (n=27) formed

View Article Online
DOI: 10.1039/D2NR00556E

fluctuating channels of varying conductance in the membrane, indicating non-uniform unstable assemblies **(Fig. 6a and fig. S7)**. Furthermore, the fluctuation increased with increasing voltages, with the ion conductance ranging from 0.05 nS to 2 nS **(Fig. 6a and fig. S7).** In some instances, the peptide formed transient pores with ion current spikes of short duration and low amplitude (<+50 pA). Notably, at higher voltages (+200 mV), we observed a drop in the ion current to almost zero (n=9), most likely indicative of the unstable peptide oligomers leaving the bilayer due to dissociation **(Fig. 6a and fig. S7**). Based on these results, we hypothesize that due to the lack of anchorage provided by the tryptophan, the peptide could not insert into the bilayer in a stable conformation to form well-defined pores. We suggest that tryptophan mutant non-specifically ruptures **(Fig 6a)** the membrane-like antimicrobial peptides.

Unlike the tryptophan mutant, the proline mutant pPorU-P29C (**Fig. 6b and fig. S8**) inserted into the membrane rapidly, emphasizing the importance of tryptophan in membrane insertion and anchorage. At +200 mV, pPorU-P29C peptides formed pores in the membrane (n=20) with two distinct channel properties. The first pore type produced a very low current state (less than 10 pA) with intermittent transient noisy spikes, most likely indicating the initial binding of peptides with the membrane. This particular state is similar to the low conductance state exhibited by the WT pPorU during low voltage interactions (**Fig. 6b and fig. S8**). The second type pore produced a slightly fluctuating state with an increased conductance of ~2 nS, similar to the second intermediate state formed by WT pPorU. In some instances, the pore produced noisy conductance states, although a stable conductance state is generally observed. In contrast to the tryptophan mutant, the proline mutant remained in the membrane for longer durations, demonstrating considerably stable oligomer formation in the membrane environment (**Fig. 6b and fig. S8**). Interestingly, the proline mutant did not form the large stable conductance channels (5 nS in 1M

View Article Online
DOI: 10.1039/D2NR00556E

KCl) as seen for WT pPorU. We suggest that this particular mutant is trapped in the intermediate steps indicating partial oligomer conformation formation. Thus, proline could be playing a role in the transition of the peptide monomers and oligomers to the final stable conformation through the different intermediate states. Importantly previous studies support the role of proline in controlling the flexibility of alpha-helical peptides in the membrane environment.[45-47] Remarkably, the drastic difference in the single-channel electrical and biophysical properties of WT and pPorU mutants demonstrates the sequence specificity of alpha-helical peptide pores. The major change in alpha-helical pore's structural and functional properties with a single amino-acid substitution affirms the exciting features of alpha-helical pore assemblies. Accordingly, the flexibility and tunability of alpha-helices associated with balancing their self-assembly and membrane solubility are essential for assembling defined structures. Previously, we have shown that pPorA self-assembled as an octamer in the SDS PAGE and gel extracted octamer readily inserted into planar lipid bilayers and formed stable cation-selective pores.[32, 33, 48] In contrast to pPorA, the pPorU peptides run on an SDS-PAGE gel formed only monomers, indicating the absence of self-assembled stable oligomers.[32] This drastic difference in the assembly mechanism of pPorU and pPorA demonstrates the sequence specificity of alpha-helical peptide pore formation in planar lipid bilayers. Similar to pPorA, the pPorU peptides formed cation-selective pores that were blocked by cationic cyclic oligosaccharides indicating the presence of predominant negatively charged residues similar to pPorA. Additionally, we suggest that the presence of a tryptophan residue in the middle of the pPorU sequence along with proline and a cluster of phenylalanine residues gives specificity in the formation of large-conductance pores. We also demonstrate their potential as a nanopore sensor for sensing complex macromolecules as the demand for developing superior pores continues. For

View Article Online
DOI: 10.1039/D2NR00556E

instance, these large-diameter pores can be applied for single-molecule sensing of large analytes, including amyloid structures, complex nucleic acids and polysaccharides.[25, 49]

Molecular dynamics simulations and model for pore formation by pPorU peptides:

So far, we have elucidated the assembly pathway of the peptide pore pPorU using single-channel electrical recordings supported by the rationally designed mutants. We used molecular dynamics simulations to address why small sequence changes make a difference in single-channel properties and subsequently investigate the specificity in forming the large pores. Through the extent of the equilibrations and simulations, the WT pPorU and two mutational variant pores sustained semi-regular hexagonal arrangements, with the most stable feature in all three structures being a well-conserved network of inter-peptide salt bridges between Asp 19 and Lys 23 of neighboring peptides. Beyond this, however, MD simulations indicate significant differences among the propensity of the different variants to sustain coherent pore-like structures in the vicinity of the pore mouths **(Fig. 6c and fig. S9).** Trp 17 proves to be a crucial determinant of pore viability and pPorU W17C pore structure tends to degenerate more irregularly. This destabilization illustrates the stable role of Trp 17 in anchoring a series of pi-stacking arrangements that are crucial to preserving a regular series of inter-peptide interactions within the N-terminal region of the pore **(Fig. 6c and fig. S9).** Specifically, Trp 17 on one peptide generally has a favorable interaction with a Phe 8 of a neighboring peptide, which, in turn, pi-stacks with Phe 6 on the first peptide. Substituting Cysteine in place of Trp 17 negates the inter-peptide coupling with Phe 8, consequently, ceases to stabilize Phe 6. The loss of these contacts produces a general lack of pore integrity for the pPorU W17C peptide.

View Article Online
DOI: 10.1039/D2NR00556E

Nevertheless, the significant lipophilicity inherent in the pPorU W17C peptide likely ensures that it will interact with cell membranes, but this is unlikely to translate into the formation of stable membrane-spanning pores (**Fig. 6a, 6c and fig. S9).** Notably, pPorU P29C pore exhibits substantial loosening of inter-peptide contacts in the C-terminal region of the pore. Notably, the native form sustains a modest number of inter-peptide H-bonds within the C-terminal region via associations between Asn 30 and Gln 33. Therefore, the mutation of Pro 29 to Cysteine disrupts nearly all of these C-terminal contacts, replacing the inter-peptide H-bonds with intra-peptide coupling **(Fig. 6b, 6c and fig. S9).** Without these pore-stabilizing features, the C-terminal segments display amphiphilicity, with appreciable lipophilic surfaces that tend to maximize contacts with lipids. This leads to a pPorU P29C pore that fans out into a broader structure lacking the barrel shape of a stable membrane pore. The importance of Pro 29 in sustaining inter-peptide H-bonds is interesting since proline does not, in itself, offer opportunities for side-chain H-bonding coupling **(Fig. 6b, 6c and fig. S9).** Proline is valuable for pore stability because it kinks the peptide helix in a manner that induces the C-terminus of one peptide to more closely approach one of its immediately adjacent peptide neighbors, thus favoring inter-peptide N30 and Q33 H-bonds over intra-peptide associations.

Our model for the pore assembly based on electrical recordings is that individual pPorU peptide monomers insert into the bilayer to form an intermediate (I) state. The intermediate state showed a noisy well-defined conductance state, revealing membrane association of the peptides and most likely forming the incomplete pores. Finally, (I) state transforms into a fully opened stable conductance state, revealing the assembly of complete stable pores (L), which remained in the lipid membrane in the same conformation for longer durations **(Fig. S10).** Remarkably, we show

View Article Online
DOI: 10.1039/D2NR00556E

that this particular model of stable pore assembly is limited to high voltages, whereas unstable noisy intermediate state pores are formed at lower voltages. We also comment on the potential role of specific amino acids in the pore's transition via different intermediates to the large conductance pore. The C-terminal D4 domain of the 340-kDa Wza polysaccharide transporters is an octameric alpha-helix barrel that spans the outer membrane of various Gram-negative bacteria.[28] Previous studies have shown that 35-amino acid, synthetic D4 peptides corresponding to the components of this domain insert into lipid bilayers to form pores via precursor state, low conductance and high conductance state. Interestingly, in contrast to pPorU pores, the cWza pore transitions were reversible.[28] pPorU also exhibited unusually high conductance of ~5.0 nS, whereas fully open cWza exhibited ~0.9 nS conductance and did not remain in the bilayer as oligomers disassemble to monomeric peptide conformations. Based on this, we suggest that the intermediate steps observed during pPorU pores could represent membrane binding, different oligomer conformations and pore states proposed in the assembly of PFTs.[7] This understanding could provide a better understanding of their assembly pathway and reveal amino-acid targets that could specifically hamper, binding or transition of the PFTs, trapping them in their non-toxic states. This could also lead to the development of more effective therapeutics against bacteria that produce membrane attacking PFTs.[7]

Conclusion

Understanding the molecular assembly mechanism of membrane-active peptides and proteins is very challenging. We characterized the assembly of short alpha-helical peptide pores based on naturally occurring alpha-helical porins using single-channel electrical recordings. We elucidated the intermediate steps involved in the pore assembly from peptide monomers to a large pore

View Article Online
DOI: 10.1039/D2NR00556E

oligomer in the lipid membrane. Furthermore, we characterized various mutants to decipher the critical amino acids' role in the structural assembly pathway. We suggest that the understanding assembly mechanism of simple alpha-helical peptide pores sheds light on the mechanism of clinically relevant pore-forming proteins, including membrane-active toxins and antimicrobial peptides. This new class of alpha-helical pores showing very large conductance can be used for nanopore technology and would allow the design of pores for biotechnology applications.

Experimental section

Single-Channel Electrical Recordings.

Planar lipid bilayer recordings were carried out by using bilayers of 1,2-diphytanoyl-snglycero-3-phosphocholine (DPhPC, Avanti Polar Lipids) formed across an aperture (~100 μm in diameter) in a 25-μm thick polytetrafluoroethylene (Teflon) film (Goodfellow, Cambridge), which separated the apparatus into cis and trans compartments (600 μL each).[50] Bilayers were formed by first pretreating the aperture with hexadecane in n-pentane (2 μL, 5%) on each side. Both compartments were then filled with the electrolyte solution (1 M KCl, 10 mM HEPES, pH 7.4), and DPhPC in n-pentane (2 μL, 5 mg mL^{-1}) was added to both sides; after that, the solvent evaporated. A bilayer was formed when the electrolyte was raised, bringing the two lipid surface monolayers together at the aperture. The pPorU pores were formed by adding a peptide solution (cis side) in 0.1% DDM (0.1 μL, 25 μM) under an applied potential of +200 mV. DTT (1 μM) was added to the cis side to facilitate the insertion of cysteine mutants of pPorU peptides into the lipid bilayer. The cis compartment was connected to the grounded electrode, and the trans compartment was attached to the working electrode. A potential difference was applied through a pair of Ag/AgCl electrodes, set in 3% agarose containing 3.0 M KCl. The current was amplified using an Axopatch 200B

View Article Online
DOI: 10.1039/D2NR00556E

amplifier, digitized with a Digidata 1550B, and recorded with pClamp 10.6 acquisition software (Molecular Devices, CA) with a low-pass filter frequency of 2 kHz and a sampling frequency of 10 kHz. pPorU blocking by cationic cyclodextrins was quantified using a statistical analysis of the pore in its unblocked and blocked states. These data were recorded with a low-pass filter frequency of 10 kHz and a sampling frequency of 50 kHz to resolve blocking events up to 100 μS. The data were analyzed and prepared for presentation with pClamp (version 10.6, Molecular Devices, CA) and Origin.

Circular Dichroism Spectroscopy.

Circular dichroism spectra were obtained using Jasco J-810 spectropolarimeter. Peptide samples were prepared as 25 μM solutions in phosphate-buffered saline (PBS, 8.2 mM sodium phosphate, 1.8 mM potassium phosphate, 137 mM sodium chloride, and 2.7 mM potassium chloride at pH 7.4) with 1% DDM, 1% Genapol or 1% SDS. Spectra were collected using a 1 mm path length quartz cuvette at 20 °C. For each data set (in deg), baselines from the same buffer and cuvette were subtracted, and then data points were normalized for amide bond concentration and path length to give mean residue ellipticity (MRE; deg cm^2 $dmol^{-1}$ res^{-1}).

Molecular Dynamics Simulations:

Molecular dynamic simulations were performed to assess the conformational stability of two specific point mutations (W17C and P29C) of membrane-bound hexameric pPorU compared with the native pPorU pore. The pore structure's initial approximation entailed a bundle of six regularly helical pPorU monomers assembled as an unstrained barrel of membrane-spanning length. From this initial structure, prospective structures for the W17C and P29C mutants were constructed by editing the native pPorU structure in PyMol using the mutagenesis wizard. Using the on-line Charmm GUI[51], each resulting pore was embedded into a bilayer composed of POPC, POPE and

View Article Online
DOI: 10.1039/D2NR00556E

POPG lipids in a 3:1:1 ratio, with cytoplasmic and extracellular buffers (extending 15.0 Å above and below the bilayer) composed of water, 67 K+ ions and 21 Cl- ions, thus comprising material and charge densities that reasonably approximate the dielectric within proximity to a POPC+POPE+POPG membrane. To derive a physically realistic starting point from which to assess the relative stability of the three pore models, extensive restrained constant pressure structural refinements were carried out in NAMD [52], representing the structures via the Charmm 3.6 force field.[53] Given a thermostatic temperature of 303.15K, an initial 10,000 step relaxation was performed using quadratic positional restraints on all protein backbone atoms via a restraint scaling factor of 10.0. A second 12,500 step restraint relaxation was then conducted on the resulting system, using a scaling factor of 5.0. Four further relaxations were then conducted (of respective lengths 12,500, 25,000, 25,000, and 25,000 steps) with restraint scaling factors diminishing according to the progression 2.5, 1.0, 0.5 and 0.1). A final production simulation was then run for 4.0 nS, at constant pressure, with no positional restraints.

Supporting Information

Materials, text, table and Fig. S1–S10 are referred to in the Supplementary Information.

Conflicts of interest

There are no conflicts to declare.

Author Contributions

NP and SKR performed the single-channel current recordings. NP and SKR analyzed the single-channel data. GN assisted in data analysis. KRM, NP and SKR designed the experiments and wrote the paper. KRM supervised the study.

View Article Online
DOI: 10.1039/D2NR00556E

Acknowledgments

This work was supported by the Ramalingaswami Re-entry fellowship of the Department of Biotechnology, Government of India (BT/RLF/Re-entry/49/2014). KRM acknowledges the research grant awarded by Science & Engineering Research Board (SERB), Department of Science and Technology, Government of India (CRG/2021/000622) and the research grant awarded by the Department of Biotechnology, Government of India (BT/PR34466/BRB/10/1830/2019) for supporting this work. We thank Dr. Gerald Lushington for assisting with Molecular dynamics simulations. NP is supported by the University Grants Commission, Government of India. SKR is supported by Senior Research Fellowship from the Indian Council of Medical Research (5/3/8/9/ITR-F/2020).

References:

1. G. von Heijne, *Nat. Rev. Mol. Cell. Biol.*, 2006, **7**, 909-918.
2. H. Bayley and L. Jayasinghe, *Mol. Membr. Biol.*, 2004, **21**, 209-220.
3. L. Sun, K. Hristova and W. C. Wimley, *Nanoscale*, 2021, **13**, 12185-12197.
4. M. Dal Peraro and F. G. van der Goot, *Nat. Rev. Microbiol.*, 2016, **14**, 77-92.
5. C. Leung, N. V. Dudkina, N. Lukoyanova, A. W. Hodel, I. Farabella, A. P. Pandurangan, N. Jahan, M. Pires Damaso, D. Osmanovic, C. F. Reboul, M. A. Dunstone, P. W. Andrew, R. Lonnen, M. Topf, H. R. Saibil and B. W. Hoogenboom, *eLife*, 2014, **3**, e04247.
6. H. Bayley, *Nature*, 2009, **459**, 651-652.
7. R. J. C. Gilbert, H. Bayley and G. Anderluh, *Philos. Trans. R. Soc. Lond. B Biol. Sci.*, 2017, **372**.
8. J. R. Thompson, B. Cronin, H. Bayley and M. I. Wallace, *Biophys. J.*, 2011, **101**, 2679-2683.
9. D. Stoddart, M. Ayub, L. Hofler, P. Raychaudhuri, J. W. Klingelhoefer, G. Maglia, A. Heron and H. Bayley, *Proc. Natl. Acad. Sci. U. S. A.*, 2014, **111**, 2425-2430.

View Article Online
DOI: 10.1039/D2NR00556E

10. C. Leung, A. W. Hodel, A. J. Brennan, N. Lukoyanova, S. Tran, C. M. House, S. C. Kondos, J. C. Whisstock, M. A. Dunstone, J. A. Trapani, I. Voskoboinik, H. R. Saibil and B. W. Hoogenboom, *Nat. Nanotechnol.*, 2017, **12**, 467-473.

11. H. Bayley, L. Jayasinghe and M. Wallace, *Nat. Struct. Mol. Biol.*, 2005, **12**, 385-386.

12. H. E. Autzen, D. Julius and Y. Cheng, *Curr. Opin. Struct. Biol.*, 2019, **58**, 259-268.

13. P. L. Frederix, P. D. Bosshart and A. Engel, *Biophys. J.*, 2009, **96**, 329-338.

14. A. A. Lee, M. J. Senior, M. I. Wallace, T. E. Woolley and I. M. Griffiths, *J. R. Soc. Interface*, 2016, **13**, 20150762.

15. L. Jayasinghe and H. Bayley, *Protein Sci.*, 2005, **14**, 2550-2561.

16. L. Franceschini, M. Soskine, A. Biesemans and G. Maglia, *Nat. Commun.*, 2013, **4**, 2415.

17. M. Ayub and H. Bayley, *Curr. Opin. Chem. Biol.*, 2016, **34**, 117-126.

18. J. J. Kasianowicz, A. K. Balijepalli, J. Ettedgui, J. H. Forstater, H. Wang, H. Zhang and J. W. Robertson, *Biochim. Biophys. Acta.*, 2016, **1858**, 593-606.

19. G. Huang, K. Willems, M. Soskine, C. Wloka and G. Maglia, *Nat. Commun.*, 2017, **8**, 935.

20. C. Cao, Y. L. Ying, Z. L. Hu, D. F. Liao, H. Tian and Y. T. Long, *Nat. Nanotechnol.*, 2016, **11**, 713-718.

21. S. Majd, E. C. Yusko, Y. N. Billeh, M. X. Macrae, J. Yang and M. Mayer, *Curr. Opin. Biotechnol.*, 2010, **21**, 439-476.

22. S. Wang, Z. Zhao, F. Haque and P. Guo, *Curr. Opin. Biotechnol.*, 2018, **51**, 80-89.

23. H. Ouldali, K. Sarthak, T. Ensslen, F. Piguet, P. Manivet, J. Pelta, J. C. Behrends, A. Aksimentiev and A. Oukhaled, *Nat. Biotechnol.*, 2020, **38**, 176-181.

24. S. Howorka, *Nat. Nanotechnol.*, 2017, **12**, 619-630.

25. C. Xu, P. Lu, T. M. Gamal El-Din, X. Y. Pei, M. C. Johnson, A. Uyeda, M. J. Bick, Q. Xu, D. Jiang, H. Bai, G. Reggiano, Y. Hsia, T. J. Brunette, J. Dou, D. Ma, E. M. Lynch, S. E. Boyken, P. S. Huang, L. Stewart, F. DiMaio, J. M. Kollman, B. F. Luisi, T. Matsuura, W. A. Catterall and D. Baker, *Nature*, 2020, **585**, 129-134.

26. A. J. Scott, A. Niitsu, H. T. Kratochvil, E. J. M. Lang, J. T. Sengel, W. M. Dawson, K. R. Mahendran, M. Mravic, A. R. Thomson, R. L. Brady, L. Liu, A. J. Mulholland, H. Bayley, W. F. DeGrado, M. I. Wallace and D. N. Woolfson, *Nat. Chem.*, 2021.

View Article Online
DOI: 10.1039/D2NR00556E

27. M. Mravic, J. L. Thomaston, M. Tucker, P. E. Solomon, L. Liu and W. F. DeGrado, *Science*, 2019, **363**, 1418-1423.

28. K. R. Mahendran, A. Niitsu, L. Kong, A. R. Thomson, R. B. Sessions, D. N. Woolfson and H. Bayley, *Nat. Chem.*, 2017, **9**, 411-419.

29. J. U. Bowie, *J. Mol. Biol.*, 1997, **272**, 780-789.

30. N. H. Joh, T. Wang, M. P. Bhate, R. Acharya, Y. Wu, M. Grabe, M. Hong, G. Grigoryan and W. F. DeGrado, *Science*, 2014, **346**, 1520-1524.

31. D. N. Woolfson, *Subcell. Biochem.*, 2017, **82**, 35-61.

32. R. S. Krishnan, R. Satheesan, N. Puthumadathil, K. S. Kumar, P. Jayasree and K. R. Mahendran, *J. Am. Chem Soc.*, 2019, **141**, 2949-2959.

33. S. K. R, N. Puthumadathil, A. H. Shaji, K. Santhosh Kumar, G. Mohan and K. R. Mahendran, *Chem. Sci.,* 2020, **12**, 639-649.

34. N. Abdali, F. Younas, S. Mafakheri, K. R. Pothula, U. Kleinekathofer, A. Tauch and R. Benz, *BMC Biochem.*, 2018, **19**, 3.

35. K. A. Brogden, *Nat. Rev. Microbiol.*, 2005, **3**, 238-250.

36. C. Song, C. Weichbrodt, E. S. Salnikov, M. Dynowski, B. O. Forsberg, B. Bechinger, C. Steinem, B. L. de Groot, U. Zachariae and K. Zeth, *Proc. Natl. Acad. Sci. U. S. A.*, 2013, **110**, 4586-4591.

37. N. Puthumadathil, P. Jayasree, K. Santhosh Kumar, K. M. Nampoothiri, H. Bajaj and K. R. Mahendran, *Biomater. Sci.*, 2019, **7**, 3226-3237.

38. C. Lan, A. Stulz, N. P. F. Barthes, S. Lauw, P. Salavei, M. Jung, H. Heerklotz and M. H. Ulbrich, *Nanoscale*, 2021, **13**, 20692-20702.

39. M. Schiffer, C. H. Chang and F. J. Stevens, *Protein Eng.*, 1992, **5**, 213-214.

40. A. J. de Jesus and T. W. Allen, *Biochim. Biophys. Acta.*, 2013, **1828**, 864-876.

41. G. von Heijne, *J.Mol. Biol.*, 1991, **218**, 499-503.

42. D. J. Barlow and J. M. Thornton, *J. Mol. Biol.*, 1988, **201**, 601-619.

43. D. N. Woolfson, R. J. Mortishire-Smith and D. H. Williams, *Biochem. Biophys. Res. Commun.*, 1991, **175**, 733-737.

44. F. S. Cordes, J. N. Bright and M. S. Sansom, *J. Mol. Biol.*, 2002, **323**, 951-960.

View Article Online
DOI: 10.1039/D2NR00556E

45. D. P. Tieleman, I. H. Shrivastava, M. R. Ulmschneider and M. S. Sansom, *Proteins*, 2001, **44**, 63-72.

46. M. S. Sansom and H. Weinstein, *Trends Pharmacol. Sci.*, 2000, **21**, 445-451.

47. A. H. Andreotti, *Nat. Chem. Biol.*, 2006, **2**, 13-14.

48. N. Abdali, E. Barth, A. Norouzy, R. Schulz, W. M. Nau, U. Kleinekathofer, A. Tauch and R. Benz, *PLoS One*, 2013, **8**, e75651.

49. A. J. Scott, A. Niitsu, H. T. Kratochvil, E. J. M. Lang, J. T. Sengel, W. M. Dawson, K. R. Mahendran, M. Mravic, A. R. Thomson, R. L. Brady, L. Liu, A. J. Mulholland, H. Bayley, W. F. DeGrado, M. I. Wallace and D. N. Woolfson, *Nat. Chem.*, 2021, **13**, 643-650.

50. T. Gutsmann, T. Heimburg, U. Keyser, K. R. Mahendran and M. Winterhalter, *Nat. Protoc.*, 2015, **10**, 188-198.

51. J. Lee, X. Cheng, J. M. Swails, M. S. Yeom, P. K. Eastman, J. A. Lemkul, S. Wei, J. Buckner, J. C. Jeong, Y. Qi, S. Jo, V. S. Pande, D. A. Case, C. L. Brooks, 3rd, A. D. MacKerell, Jr., J. B. Klauda and W. Im, *J. Chem. Theory. Comput.*, 2016, **12**, 405-413.

52. J. C. Phillips, D. J. Hardy, J. D. C. Maia, J. E. Stone, J. V. Ribeiro, R. C. Bernardi, R. Buch, G. Fiorin, J. Henin, W. Jiang, R. McGreevy, M. C. R. Melo, B. K. Radak, R. D. Skeel, A. Singharoy, Y. Wang, B. Roux, A. Aksimentiev, Z. Luthey-Schulten, L. V. Kale, K. Schulten, C. Chipot and E. Tajkhorshid, *J. Chem. Phys.*, 2020, **153**, 044130.

53. J. Huang and A. D. MacKerell, Jr., *J. Comput. Chem.*, 2013, **34**, 2135-2145.